

## DDFT calibration and investigation of an anisotropic phase-field crystal model

This article has been downloaded from IOPscience. Please scroll down to see the full text article.

2011 J. Phys.: Condens. Matter 23 265005

(<http://iopscience.iop.org/0953-8984/23/26/265005>)

View [the table of contents for this issue](#), or go to the [journal homepage](#) for more

Download details:

IP Address: 134.99.64.184

The article was downloaded on 12/09/2011 at 08:56

Please note that [terms and conditions apply](#).

# DDFT calibration and investigation of an anisotropic phase-field crystal model

Muhammad Ajmal Choudhary<sup>1</sup>, Daming Li<sup>1</sup>, Heike Emmerich<sup>1</sup>  
and Hartmut Löwen<sup>2</sup>

<sup>1</sup> Lehrstuhl für Material- und Prozesssimulation, Universität Bayreuth, D-95440 Bayreuth, Germany

<sup>2</sup> Institut für Theoretische Physik II: Weiche Materie, Heinrich-Heine-Universität Düsseldorf, D-40225 Düsseldorf, Germany

E-mail: [ajmal.choudhary@uni-bayreuth.de](mailto:ajmal.choudhary@uni-bayreuth.de)

Received 17 January 2011, in final form 18 April 2011

Published 13 June 2011

Online at [stacks.iop.org/JPhysCM/23/265005](http://stacks.iop.org/JPhysCM/23/265005)

## Abstract

The anisotropic phase-field crystal model recently proposed and used by Prieler *et al* (2009 *J. Phys.: Condens. Matter* **21** 464110) is derived from microscopic density functional theory for anisotropic particles with fixed orientation. Its morphology diagram is also explored. In particular we have investigated the influence of anisotropy and undercooling on the process of nucleation and microstructure formation from the atomic to the microscale. To that end numerical simulations were performed varying those dimensionless parameters which represent anisotropy and undercooling in our anisotropic phase-field crystal model. The results from these numerical simulations are summarized in terms of a morphology diagram of the stable state phases. These stable phases are also investigated with respect to their kinetics and characteristic morphological features.

(Some figures in this article are in colour only in the electronic version)

## 1. Introduction

In the late 1970s Swift and Hohenberg formulated an amplitude approach to describe systems where the stable states are periodic such as, for example, the case for Rayleigh–Bénard convection [1]. More recently this idea has been taken up by the materials science community to model crystals at the atomic scale. Elder *et al* proposed a functional for a scalar dimensionless field  $\phi$  of the form

$$F = \int_V \left( \frac{1}{2} \phi [(q_0^2 + \nabla^2)^2 - \varepsilon] \phi + \frac{1}{4} \phi^4 \right) dr, \quad (1)$$

with two phenomenological parameters  $q_0$  and  $\varepsilon$  and a corresponding dynamical equation

$$\frac{\partial \phi}{\partial t} = \nabla^2 \frac{\delta F}{\delta \phi} \quad (2)$$

for this purpose [2]. Since its introduction, this phase-field crystal (PFC) method [2–6] has emerged as a computationally efficient alternative to molecular dynamics (MD) simulations

for problems where the atomic and the continuum scale are tightly coupled. The reason is that it operates for atomic length scales and diffusive timescales. Thus for a simple application such as diffusion in gold or copper it runs  $10^6$ – $10^8$  times faster than the corresponding MD calculation [7]. In that sense it provides, from the point of view of multiscale materials modelling, an interesting link between the traditional phase-field method and MD. Moreover, a connection between the classical density functional theory of freezing and PFC modelling was identified in [4, 8]. Thereby a second theoretical foundation besides the Swift–Hohenberg amplitude equation approach could be established. Essentially it motivates the application of PFC models also for spatially non-uniform non-periodic states.

Recently the PFC method has been applied to a variety of different growth phenomena. One of its interesting features is that other than the phase-field method, in which elasticity explicitly needs to be integrated in the functional to be taken into account [9], it includes elastic effects inherently. Thus it allows one to simulate, for example, features of crack propagation [4] and plasticity [3, 10] from the atomic to the

microscale. To model the elastic behaviour of different kinds of materials, the parameters of the PFC model equation can be adjusted to match the elastic moduli of a given experimental system. However, in its most simplistic form, in which it is a reformulation of the Swift–Hohenberg equation [1] with a conserved dynamics as introduced by Elder *et al* [2, 3], the Poisson ratios which can be modelled are restricted to 1/3 (in the one mode approximation). Moreover, since in the simplistic PFC model the material is defined by only three parameters, it is restricted with respect to the crystal lattice structures which it can describe as well. These are triangular symmetries in two dimensions and *BCC* symmetry in three dimensions [11, 12]. Another crystal symmetry applying to protein crystals in a membrane could be obtained by including higher order correlation functions [13]. Moreover, liquid crystals have been simulated by combining the original PFC equation with an orientational field [14, 16, 15].

In [17] we followed the above direction to extend the phase field to apply to a larger class of condensed matter systems taking a different route: we derived a generalized PFC model for isotropic as well as anisotropic crystal lattice systems of arbitrary Poisson ratios as well as condensed matter systems built up from non-spherical units such as, for example, anisotropic colloids and liquid crystals. To this end we extended the simplest PFC model proposed by Elder [2] to a conservative, anisotropic Langevin equation and applied it to the heterogeneous nucleation of colloids at a wall.

Whereas our previous work [17] was devoted to a mere introduction of our model and its application to heterogeneous nucleation at a wall, here we show for the first time how its parameters can be derived from dynamical density functional theory (DDFT) (see section 2). Further we report for the first time in detail on its morphology diagram. To do so, we proceed as follows. First we give a thorough derivation of our anisotropic phase-field model based on the DDFT in section 2. We then—after a brief summary of the model in section 2—study the influence of anisotropy and undercooling on the morphology of the final states. We analyse these morphologies and summarize our results in terms of a morphology diagram in section 4. Finally we conclude with a summary and an outlook of our study in section 5.

## 2. The anisotropic phase-field crystal model

### 2.1. The model

Currently PFC modelling is widely used to predict crystal nucleation growth and to model microstructural pattern formation during different physical phenomena such as solidification. As usual, the PFC model used in this study is based on a free energy functional  $F[\phi(r, t)]$  of the phase field  $\phi(r, t)$  and a dynamical equation which represents the time evolution of the phase field. In this PFC model, the periodic nature of a crystal lattice is incorporated by using a free energy functional which is minimized by a periodic density field. The equation of motion used in this model was introduced in [2] for the case of the simplest phase-field crystal (SPFC) model, and

is given by

$$\rho \frac{\partial \phi}{\partial t} = \Delta \{ [(q_0^2 + \Delta)^2 - \epsilon] \phi + \phi^3 \}. \quad (3)$$

Here,  $q_0$  and  $\epsilon$  are constants. In order to simplify the model, a dimensionless parameter  $\tau$  is introduced which is defined as

$$\tau = -(q_0^2 - \epsilon). \quad (4)$$

In our model  $\tau$  represents undercooling in the same manner as  $r$  is defined in [3]; therefore,  $\tau$  can be written as

$$\tau \propto \Delta T. \quad (5)$$

The anisotropic version of the phase-field crystal model (APFC) originally introduced in [18] is used in this study. This PFC model is basically an extension of the SPFC model which is derived in [19]. The APFC model is capable of simulating isotropic and anisotropic crystal lattice systems of any arbitrary Poisson ratio as well as condensed matter systems such as colloids and liquid crystals. The free energy functional used in this model is given by

$$F = \int_V \left( \frac{1}{2} \phi \left[ -\tau + a_{ij} \frac{\partial^2}{\partial x_i \partial x_j} + b_{ijkl} \frac{\partial^4}{\partial x_i \partial x_j \partial x_k \partial x_l} \right] \phi + \frac{1}{4} c \phi^4 \right) dr, \quad (6)$$

where  $a_{ij}$  is a symmetric matrix and  $b_{ijkl}$  is a fourth rank tensor with the symmetry of an elastic tensor:  $i \leftrightarrow j, k \leftrightarrow l, (i, j) \leftrightarrow (k, l)$ . From the free energy functional defined in equation (6), the corresponding Langevin differential equation of motion for an anisotropic lattice system can be written as follows:

$$\rho \frac{\partial \phi}{\partial t} = \Delta \left( \left[ -\tau + a_{ij} \frac{\partial^2}{\partial x_i \partial x_j} + b_{ijkl} \frac{\partial^4}{\partial x_i \partial x_j \partial x_k \partial x_l} \right] \phi + c \phi^3 \right). \quad (7)$$

### 2.2. Derivation of the anisotropic phase-field crystal model from dynamical density functional theory

The coefficients occurring in the APFC model proposed in [17] can be derived from microscopic density functional theory [20–23]. Here we follow a similar route as proposed recently by van Teeffelen *et al* [8] for radially symmetric interactions. We generalize this route here to anisotropic interactions.

We assume that the anisotropic colloids are completely aligned in space. Cartesian coordinates  $\mathbf{r} = (x_1, x_2, \dots, x_d)$  will be used in the following derivation, where  $d$  denotes the spatial dimension. By scaling, hard ellipsoids with fixed orientation are formally equivalent to hard-sphere systems. This is no longer true if the interactions are soft and involve an explicit energy scale. The interaction pair potential between two aligned particles is  $u(\mathbf{r})$ . The latter function is anisotropic, in general, i.e. it does not only depend on  $|\mathbf{r}|$ . Other examples for these anisotropic interactions with fixed orientations are oriented hard spherocylinders [24] and charged rods [25, 26], anisotropic Gaussian potentials [27],

board-like colloidal particles [28], colloidal molecules [29], as well as patchy colloids [30] and proteins [31, 32]. Henceforth inversion symmetry is assumed

$$u(-\mathbf{r}) = u(\mathbf{r}). \quad (8)$$

The DDFT for anisotropic situations [33] is now generalized from the isotropic case as follows. The dynamical evolution of the time-dependent one-particle density field  $\rho(\mathbf{r}, t)$  is

$$\dot{\rho}(\mathbf{r}, t) = (k_B T)^{-1} \nabla \cdot \left[ \mathcal{D} \rho(\mathbf{r}, t) \nabla \frac{\delta F[\rho(\mathbf{r}, t)]}{\delta \rho(\mathbf{r}, t)} \right]. \quad (9)$$

Here  $k_B T$  is the thermal energy, and  $\nabla = (\partial/\partial x_1, \partial/\partial x_2, \dots, \partial/\partial x_d)$  is the  $d$ -dimensional gradient.  $\mathcal{D} = \text{diag}(D_1, D_2, \dots, D_d)$  denotes the diagonalized diffusion tensor with the anisotropic short-time translational diffusivities of the anisotropic particle. For a given (hydrodynamic) shape of the particle, explicit expressions for  $D_i$  are available [34, 35]. Furthermore, in equation (9),  $F[\rho(\mathbf{r}, t)]$  is the equilibrium density functional which can be split as

$$F[\rho(\mathbf{r})] = F_{\text{id}}[\rho(\mathbf{r})] + F_{\text{ex}}[\rho(\mathbf{r})] + F_{\text{ext}}[\rho(\mathbf{r})], \quad (10)$$

where

$$F_{\text{id}}[\rho(\mathbf{r})] = k_B T \int d\mathbf{r} \rho(\mathbf{r}) \{ \ln[\rho(\mathbf{r}) \Lambda^d] - 1 \}, \quad (11)$$

with  $\Lambda$  denoting the thermal de Broglie wavelength. The external part involves an external one-body potential  $V(\mathbf{r}, t)$  and is given by

$$F_{\text{ext}}[\rho(\mathbf{r})] = \int d\mathbf{r} \rho(\mathbf{r}) V(\mathbf{r}, t). \quad (12)$$

Finally, the excess part,  $F_{\text{ex}}[\rho(\mathbf{r})]$ , embodies the nontrivial correlations between the particles and must be further approximated. Henceforth we assume small deviations of the inhomogeneous density profile around a homogeneous reference density  $\rho$ . In this limit, the leading approximation for  $F_{\text{ex}}[\rho(\mathbf{r})]$  is given by the Ramakrishnan and Yussouff [36] expression:

$$F_{\text{ex}}[\rho(\mathbf{r})] \simeq F_{\text{ex}}(\rho) - \frac{k_B T}{2} \int \int d\mathbf{r} d\mathbf{r}' \Delta \rho(\mathbf{r}) \Delta \rho(\mathbf{r}') c_0^{(2)}(\mathbf{r} - \mathbf{r}'; \rho), \quad (13)$$

where  $c_0^{(2)}(\mathbf{r} - \mathbf{r}'; \rho)$  is the anisotropic direct correlation function of the fluid at density  $\rho$  which possesses the same symmetry as the underlying pair potential  $u(\mathbf{r})$ . In particular, it is inversion symmetric

$$c_0^{(2)}(-\mathbf{r}, \rho) = -c_0^{(2)}(\mathbf{r}, \rho). \quad (14)$$

Moreover,  $\Delta \rho(\mathbf{r}) = \rho(\mathbf{r}) - \rho$ . In Fourier space equation (13) reads

$$\mathcal{F}_{\text{ex}}[\rho(\mathbf{r})] = F_{\text{ex}}(\rho) - \frac{k_B T (2\pi)^d}{2} \int d\mathbf{k} \Delta \tilde{\rho}(\mathbf{k}) \Delta \tilde{\rho}(-\mathbf{k}) \tilde{c}_0^{(2)}(\mathbf{k}, \rho), \quad (15)$$

with  $\tilde{\sim}$  denoting a Fourier transform. We now expand the direct correlation function  $c_0^{(2)}(\mathbf{k}, \rho)$  in terms of  $\mathbf{k}$  around  $\mathbf{k} = 0$ .

(Alternatively fitting procedures can be used, e.g. around the first peak of  $c_0^{(2)}(\mathbf{k}, \rho)$ .) This leads to the Taylor expansion in Fourier space

$$\tilde{c}_0^{(2)}(\mathbf{k}, \rho) = \hat{C}_0 + \sum_{i,j=1}^d a_{ij} k_i k_j + \sum_{i,j,k,l=1}^d b_{ijkl} k_i k_j k_k k_l + \dots, \quad (16)$$

corresponding to a gradient expansion in real space. The inversion symmetry equation (14) enforces the vanishing of all odd orders. Possible additional symmetries in the shape of the particles will lead to corresponding restrictions on the tensorial coefficients  $a_{ij}$  and  $b_{ijkl}$ , as discussed below.

Inserting this expansion into equation (9), one gets

$$\begin{aligned} \dot{\rho}(\mathbf{r}, t) = & \nabla \cdot \mathcal{D} \nabla \rho(\mathbf{r}, t) + \nabla \cdot \mathcal{D} \nabla \left[ (k_B T)^{-1} V(\mathbf{r}, t) \right. \\ & - \left( \hat{C}_0 - \sum_{i,j=1}^d a_{ij} \frac{\partial^2}{\partial x_i \partial x_j} \right. \\ & \left. \left. + \sum_{i,j,k,l=1}^d b_{ijkl} \frac{\partial^4}{\partial x_i \partial x_j \partial x_k \partial x_l} \right) \rho(\mathbf{r}, t) \right]. \end{aligned} \quad (17)$$

If one further uses the constant mobility approximation,  $\rho(\mathbf{r}, t) = \rho$ , in front of the functional derivative in equation (9) and if one approximates

$$\begin{aligned} F_{\text{id}}[\rho(\mathbf{r})] \approx & k_B T \rho \int d\mathbf{r} \left\{ \frac{1}{2} \phi(\mathbf{r}, t)^2 - \frac{1}{6} \phi(\mathbf{r}, t)^3 \right. \\ & \left. + \frac{1}{12} \phi(\mathbf{r}, t)^4 - \text{const.} \right\} \end{aligned} \quad (18)$$

with  $\phi(\mathbf{r}, t) = \Delta \rho(\mathbf{r}, t)/\rho$ , one arrives at

$$\begin{aligned} \dot{\phi}(\mathbf{r}, t) = & \rho \nabla \cdot \mathcal{D} \nabla \left[ \phi(\mathbf{r}, t) - \frac{1}{2} \phi(\mathbf{r}, t)^2 + \frac{1}{3} \phi(\mathbf{r}, t)^3 \right. \\ & + (k_B T)^{-1} V(\mathbf{r}, t) - \rho \left( \hat{C}_0 - \sum_{i,j=1}^d a_{ij} \frac{\partial^2}{\partial x_i \partial x_j} \right. \\ & \left. \left. + \sum_{i,j,k,l=1}^d b_{ijkl} \frac{\partial^4}{\partial x_i \partial x_j \partial x_k \partial x_l} \right) \phi(\mathbf{r}, t) \right]. \end{aligned} \quad (19)$$

This exactly reduces to the anisotropic phase-field model as used in [17] for the special case  $d = 2$ ,  $\mathcal{D} = D_0 \mathbf{1}$ , and a neglected cubic term in the ideal gas functional expansion in equation (18). As a remark, the latter was retained in other variants of the PFC model [4, 37].

Concluding this section, the APFC model as used in [17] can be derived and justified from DDFT. The derivation points, however, to more realistic approximations for anisotropic diffusivities. Furthermore, if equation (18) is used, some approximations can be avoided, but these were not found to change the results significantly for spherical interactions [8].

### 2.3. Phenomenological symmetry considerations

We finally present phenomenological symmetry arguments for the expansion coefficients  $a_{ij}$  and  $b_{ijkl}$  of the APFC model. First we assume that the orientation of the fixed particles is set by a single unit vector  $\vec{E}$  only which is invariant under space inversion ( $\vec{r} \rightarrow -\vec{r}$ ). This is the case for  $d = 2$  and for rotationally symmetric particles in  $d = 3$ . Then,

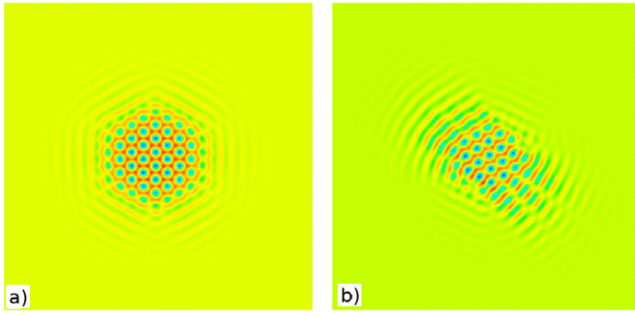


**Figure 1.** Simulation results of crystal growth calculated for  $\tau = -3/4$  with (a)  $s = 0$  (isotropic case) and (b)  $s = 0.125$  (anisotropic case). All other parameters are chosen as given in section 3. As expected, the isotropic case shows a symmetric morphology.

any gradient term in the scalar free energy functional must involve an even number of gradients due to space inversion symmetry. Rotational symmetry of space then requires that only combinations of  $\vec{E} \cdot \vec{\nabla}$  and  $\vec{\nabla} \cdot \vec{\nabla}$  are nonvanishing in the functional. Therefore the only possibility for physically relevant gradient terms is

$$\sum_{i,j=1}^d a_{ij} \frac{\partial^2}{\partial x_i \partial x_j} = \lambda_1 (\vec{E} \cdot \vec{\nabla})^2 + \lambda_2 \Delta \quad (20)$$

and

$$\sum_{i,j,k,l=1}^d b_{ijkl} \frac{\partial^4}{\partial x_i \partial x_j \partial x_k \partial x_l} = \lambda_3 (\vec{E} \cdot \vec{\nabla})^4 + \lambda_4 (\vec{E} \cdot \vec{\nabla})^2 \Delta + \lambda_5 \Delta^2, \quad (21)$$

where  $\lambda_1, \lambda_2, \lambda_3, \lambda_4,$  and  $\lambda_5$  are scalar prefactors. This reduces the number of independent degrees of freedom in  $a_{ij}$  and  $b_{ijkl}$  down to five.

In the case where there are different fixed vectors, say  $\vec{E}$  and  $\vec{B}$ , there are correspondingly more terms allowing for more freedom in  $a_{ij}$  and  $b_{ijkl}$ . This is realized, e.g., for biaxial colloidal particles in two crossed external fields along  $\vec{E}$  and  $\vec{B}$ .

### 3. Simulation parameters

As initial condition, a square domain is defined with a sphere in the centre to initialize the nucleus. Periodic boundary conditions are used in the square box in all directions. The values used for the constant parameters are the same as defined in [17], namely  $\rho = 1$  (which sets the timescale),  $a_{11} = a_{22} = 2$ ,  $b_{1111} = b_{2222} = b_{1122} = 1$ ,  $b_{1212} = 0$  and  $c = 1$ , respectively. However, this choice of parameters does not correspond to a single field direction  $\vec{E}$  but to two crossed fields  $\vec{E}$  and  $\vec{B}$  as mentioned in section 2.3. A typical set of values for  $\tau$  and  $s$  is used for each simulation since our basic objective is to study the dependence of the stable state phase on these parameters. A simple explicit numerical scheme is used to obtain a reasonably well approximated solution. A forward Euler scheme is used for the time derivative with a sufficiently

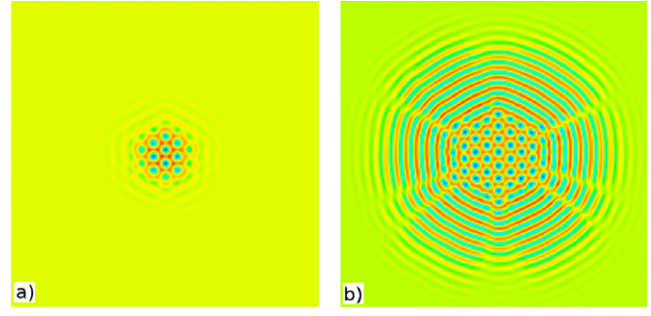


**Figure 2.** Simulation results of crystal growth after 40 000 time steps for  $s = 0$  with (a)  $\tau = -0.8$  and (b)  $\tau = -0.25$ .

small time step of  $\Delta t = 0.00075$  to ensure the stability of the scheme. The Laplace operator is approximated by using a second order difference scheme given by

$$\nabla^2 \phi = (\phi_{i+1,j} + \phi_{i-1,j} + \phi_{i,j+1} + \phi_{i,j-1} - 4\phi_{i,j}) / (\Delta x)^2. \quad (22)$$

For the following simulations  $\Delta x$  is chosen as  $\pi/4$ . Convergence of our results is ensured via convergence studies. The morphologies depicted in figures 1, 2 and 4 show simulations of  $256 \times 256$  numerical grid units. However, the morphologies in figure 5 show a simulation of  $128 \times 256$  numerical grid units.

## 4. Results and discussion

In this section we present the simulation results obtained from our studies. These simulation results demonstrate the following issues concerning nucleation and successive microstructure formation:

- (i) the effect of undercooling on crystal growth;
- (ii) the dependence of anisotropy and undercooling on the stable state phase;
- (iii) the effect of anisotropy and undercooling on the distance between the neighbouring stripes.

### 4.1. Anisotropic effects

In order to quantify the anisotropy of the material at the atomic scale, a dimensionless parameter  $s$  is introduced and is given by

$$s = -\frac{b_{1112}}{b_{1111}}. \quad (23)$$

The effect of this dimensionless parameter was studied by performing numerical simulations with  $s = 0$  and  $0.125$ . The initial and boundary conditions as well as the values for all other simulation parameters used in these simulations were the same as given in section 3. The results obtained for both cases after 30 000 time steps are shown in figure 1.

### 4.2. Undercooling effects

When a liquid is supercooled just below the melting temperature the crystal starts growing and the crystal growth is directly related to the undercooling. Depending on the formal

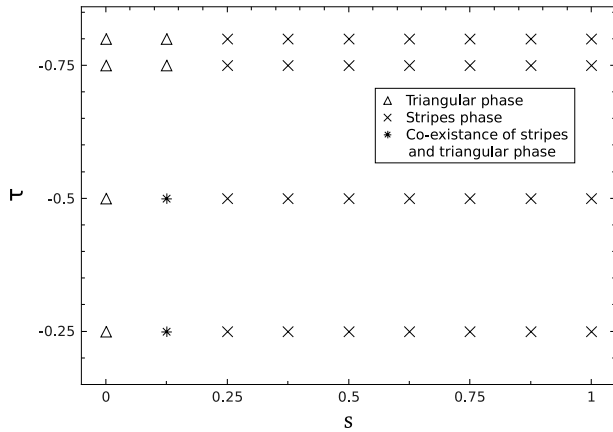


**Figure 3.** Simulation results of stable phases for the same initial conditions and different values of  $s$  and  $\tau$ .

undercooling, which quantifies the distance from the phase equilibrium line in the phase diagram, in the system the final state will have different morphologies. These are categorized and analysed here in detail to get an overview of the state phase of the APFC model given by the variables  $s$  and  $\tau$ .

Here, the APFC model was used to examine the rate of crystal growth from a supercooled liquid state. As explained above,  $\tau$  represents the undercooling in our model. A number of simulations with different values of  $\tau$  were performed for a specific  $s$  value. We used the same initial condition i.e. single solid nucleus (nucleation site) for all simulations. The results showed that the rate of crystal growth increases with an increase in the value of  $\tau$ . As an example the simulation results with  $s = 0$  and for two typical values of  $\tau$ , i.e. with  $\tau = -0.25$  and  $\tau = -0.8$  respectively, at 40 000 time steps are depicted in figure 2.

#### 4.3. Heterogeneous nucleation and crystal growth

In this section we study the dependence of a stable state phase on the anisotropy and undercooling. More specifically, we show how a stable state can be composed of different phases such as a triangular phase, a stripe phase and co-existence of stripes and a triangular phase, depending on the values of  $s$  and  $\tau$ , i.e. anisotropy and undercooling, respectively. To study these patterns we performed a number of simulations with different values of  $s$  and  $\tau$  in each simulation. However, the other parameters for all these simulations were same as described in section 4.2. The results in the form of a diagram of stable state phases are demonstrated in figure 3.

These simulation results demonstrate that the stable state phase always consists of stripes if  $s \geq 0.25$  irrespective of the  $\tau$  value. The co-existence of stripes and triangular phases is found only in the case of  $s = 0.125$  and  $\tau \geq -0.5$ , while for other values of  $s$  and  $\tau$ , the stable state consists of a triangular phase. Typical pictures of the triangular phase, stripes, and a co-existence of stripes and the triangular phase are given in figure 4.

The precise shape of the grain boundary between the two solid phases depends on the system size due to the fact that the resulting model equations of our APFC model are

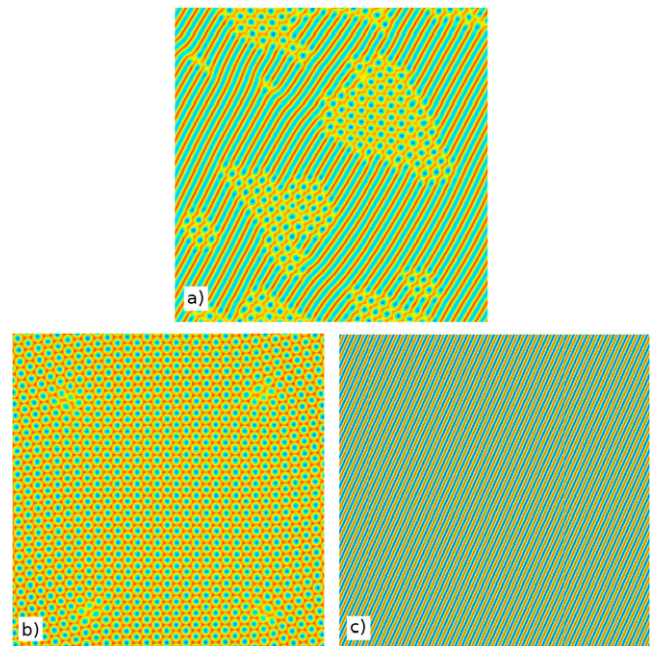


**Figure 4.** Typical stable state phases from simulations performed for (a)  $s = 0.125$  and  $\tau = -0.25$ , which result in the co-existence of stripes and a triangular phase, (b)  $s = 0$  and  $\tau = -0.75$ , which result in a triangular phase, and (c)  $s = 0.75$  and  $\tau = -0.25$ , which result in stripes.

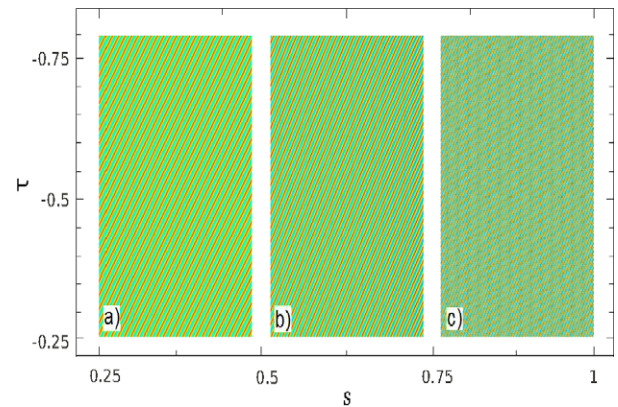


**Figure 5.** Stripe phases for different values of  $s$  and  $\tau$ . Resulting stripe phases for (a)  $s = 0.25$ , (b)  $s = 0.625$  and (c)  $s = 1$ .

not rotationally invariant just like the ones of the famous anisotropic phase-field model [38]. This might cause problems when studying, for example, several grains, and issues of their orientation with respect to each other might play an important role. The two-phase co-existence as such, however, is independent of the size of the system.

#### 4.4. Distance between the neighbouring stripes

To analyse the stripe morphology further, we studied the effect of anisotropy and undercooling on the distance between the neighbouring stripes. As discussed in section 4.3, the stable state consists of stripes when  $s \geq 0.25$  irrespective of the  $\tau$  value, as shown in figure 3. It is observed that the stripe phases obtained for different values of  $s$  are different from each other

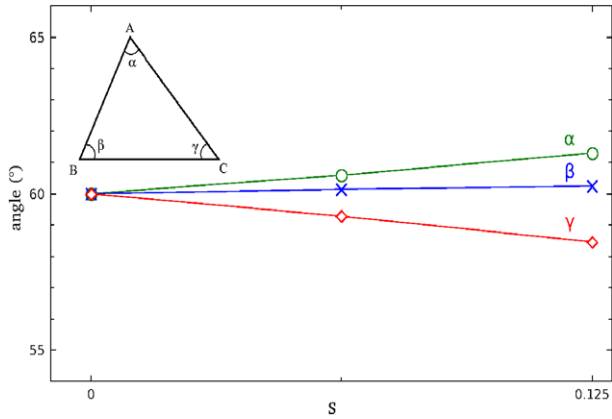


**Figure 6.** Forms of the triangles in the final triangular phase obtained for different anisotropies  $s$ .

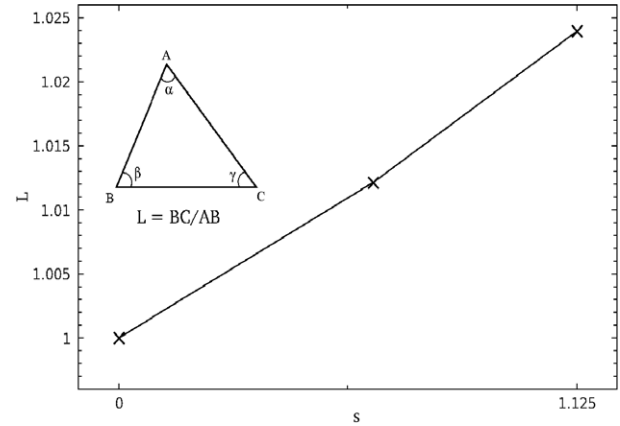


**Figure 7.** Ratio of the lengths of the longest and shortest sides of the triangles in the final triangular phase versus  $s$ .

in terms of the spacing between the neighbouring stripes in the stripe phases. However, simulations with different values of  $\tau$  in similar stripe phases. Our results reveal that the spacing between neighbouring stripes decreases with an increase in the value of  $s$ . Thus the stripe phase obtained with  $s = 1$  is much finer compared to the one obtained with  $s = 0.25$ . Further, to investigate the effect of the undercooling  $\tau$  on the stripe phase, we performed several simulations by fixing a specific value for  $s$  and varying  $\tau$ . The results show that for a specific value of  $s$ , similar stripe morphologies are obtained with different values of  $\tau$ . Figure 5 demonstrates this interesting finding for different values of  $s$  and  $\tau$ .

From the above discussion, we can conclude that the distance between neighbouring stripes decreases as we increase the value of  $s$ . However, the undercooling has no significant effect on the stable stripe phase, i.e. the stripe phases for different values of  $\tau$  are similar.

#### 4.5. Analysis of the anisotropy introduced by $s$

In this section we discuss the influence of the anisotropic factor  $s$  on the final triangular phase obtained with  $0 \leq s \leq 0.125$  and  $\tau = -0.75$ . More specifically, we analyse the form of the triangles in each of the final triangular phases. The form of a triangle is determined in terms of the three internal angles and the ratio of the lengths of the longest and shortest sides of the triangle. It is observed that the triangular phase obtained in the case of  $s = 0$ , i.e. without any anisotropy, consists of triangles with all three angles the same at  $60^\circ$  each. However, the triangular phases obtained with non-zero values of  $s$  contain triangles with dissimilar sides. The details of the angles calculated for each case are shown in figure 6.

These results demonstrate that for the isotropic case, i.e.  $s = 0$ , the final triangular phase consists of equilateral triangles. However, for the anisotropic case, i.e. non-zero values of  $s$ , the final triangular phase contains scalene triangles, i.e. no two sides are similar. The ratios of the lengths of the longest and shortest sides of the triangles calculated for each case are presented in figure 7. This underlines the capability of our APFC model to give rise to truly anisotropic morphologies.

## 5. Summary and outlook

In this paper we have presented a DDFT based derivation of the APFC model proposed by two of the authors (DL and HE) in [17] previously. Further we have investigated the state phases of this model given by variation of  $\tau$  and  $s$  to demonstrate its capacity to model structures beyond those captured by the SPFC equations originally introduced by Elder *et al* [2].

In particular we studied the influence of anisotropy and undercooling on the final states using numerical techniques to minimize the free energy functional in our model. More specifically, a number of numerical simulations were performed by using different sets of values for our dimensionless parameters  $s$  and  $\tau$  which represent anisotropy and undercooling, respectively. The results obtained from these numerical simulations were analysed. Our studies reveal the following.

- (i) The rate of crystal growth increases with increase of  $\tau$ , i.e. undercooling.
- (ii) The stable state phase consists of a stripe phase if  $s \geq 0.25$  irrespective of  $\tau$ . However, the stable state is a co-existence of stripes and a triangular phase when  $s = 0.125$  and  $\tau \geq -0.5$ , while for other values of  $s$  and  $\tau$  the stable state consists of a triangular phase.
- (iii) For  $s \geq 0.25$ , the undercooling  $\tau$  has no effect on the resulting stripe phases; however, the distance between the neighbouring stripes decreases with an increase of  $s$ .
- (iv) Triangular crystals with cells that are neither equilateral nor rhombic are possible for our anisotropic model.

In the future we plan to extend the approach to reactive systems [39] to simulate morphogenesis in such systems from the atomic to the microscale.

## Acknowledgments

We thank S van Teeffelen and T Ala-Nissila for helpful discussions. This work has been supported by the DFG through the DFG priority program SPP 1296. DL is also

supported by the National Sciences Foundation of China (Grant No. 10701056).

## References

- [1] Swift J and Hohenberg P C 1977 *Phys. Rev. A* **15** 319
- [2] Elder K R, Katakowski M, Haataja M and Grant M 2002 *Phys. Rev. Lett.* **88** 245701
- [3] Elder K R and Grant M 2004 *Phys. Rev. E* **70** 051605
- [4] Elder K R, Provatas N, Berry J, Stefanovic P and Grant M 2007 *Phys. Rev. B* **75** 064107
- [5] Stefanovic P M, Haataja M and Provatas N 2006 *Phys. Rev. Lett.* **96** 225504
- [6] Berry J, Grant M and Elder K R 2006 *Phys. Rev. E* **73** 031609
- [7] Elder K 2008 Heterogenous nucleation *Lecture Notes, Summer School of DFG Priority Program (Herzogenrath, July to Aug.)* vol 1296
- [8] van Teeffelen S, Backofen R, Voigt A and Löwen H 2009 *Phys. Rev. E* **79** 051404
- [9] Emmerich H 2003 *Contin. Mech. Thermodyn.* **15** 197
- [10] Hirouchi T, Takaki T and Tomita Y 2009 *Comput. Math. Sci.* **44** 1192
- [11] Wu K-A and Karma A 2007 *Phys. Rev. B* **76** 184107
- [12] Jaatinen A and Ala-Nissila T 2010 *J. Phys.: Condens. Matter* **22** 205402
- [13] Tupper P F and Grant M 2008 *Europhys. Lett.* **81** 40007
- [14] Löwen H 2010 *J. Phys.: Condens. Matter* **22** 364105
- [15] Wittkowski R, Löwen H and Brand H R 2010 *Phys. Rev. E* **82** 031708
- [16] Mkhonta S K, Vernon D, Elder K R and Grant M 2008 arXiv:0806.3445v2
- [17] Prieler R, Hubert J, Li D, Verleye B, Haberkern R and Emmerich H 2009 *J. Phys.: Condens. Matter* **21** 464110
- [18] Prieler R, Li D and Emmerich H 2010 *J. Cryst. Growth* **312** 1434–6
- [19] Boettinger W J, Warren J A, Beckermann C and Karma A 2002 *Annu. Rev. Mater. Res.* **32** 163
- [20] Evans R 1979 *Adv. Phys.* **28** 143
- [21] Singh Y 1991 *Phys. Rep.* **207** 351
- [22] Löwen H 1994 *Phys. Rep.* **237** 249
- [23] Löwen H 2002 *J. Phys.: Condens. Matter* **14** 11897
- [24] Bohle A M, Holyst R and Vilgis T 1996 *Phys. Rev. Lett.* **76** 1396
- [25] Löwen H 1994 *Phys. Rev. Lett.* **72** 424  
Löwen H 1994 *J. Chem. Phys.* **100** 6738
- [26] Kirchhoff T, Löwen H and Klein R 1996 *Phys. Rev. E* **53** 5011
- [27] Prestipino S and Saija F 2007 *J. Chem. Phys.* **126** 194902
- [28] van der Beek D, Davidson P, Wensink H H, Vroege G J and Lekkerkerker H N W 2008 *Phys. Rev. E* **77** 031708
- [29] Manoharan V N, Elsesser M T and Pine D J 2003 *Science* **301** 483
- [30] Bianchi E, Largo J, Tartaglia P, Zaccarelli E and Sciortino F 2006 *Phys. Rev. Lett.* **97** 168301
- [31] Allahyarov E, Löwen H, Louis A A and Hansen J-P 2002 *Europhys. Lett.* **57** 731
- [32] Allahyarov E, Löwen H, Hansen J-P and Louis A A 2003 *Phys. Rev. E* **67** 051404
- [33] Rex M, Wensink H H and Löwen H 2007 *Phys. Rev. E* **76** 021403
- [34] Tirado M M, Martinez C L and de la Torre J G 1984 *J. Chem. Phys.* **81** 2047
- [35] Löwen H 1994 *Phys. Rev. E* **50** 1232
- [36] Ramakrishnan T V and Yussouff M 1979 *Phys. Rev. B* **19** 2775
- [37] Jaatinen A, Achim C V, Elder K R and Ala-Nissila T 2009 *Phys. Rev. E* **80** 031602
- [38] Warren J A and Boettinger W J 1995 *Acta Metal. Mater.* **43** 689–703
- [39] Kutschan B, Morawetz K and Gemming S 2010 *Phys. Rev. E* **81** 036106